Solvate and protic ionic liquids from aza-crown ethers: synthesis, thermal properties, and LCST behavior

Oba, Yukiko
Okuhata, Megumi
Osakai, Toshiyuki
Mochida, Tomoyuki

(Citation)
Physical Chemistry Chemical Physics,20(5):3118-3127

(Issue Date)
2018-02-07

(Resource Type)
journal article

(Version)
Accepted Manuscript

Phys. Chem. Chem. Phys., **2018**, *20*, 3118–3127.

Solvate and protic ionic liquids from aza-crown ethers: synthesis, thermal properties, and LCST behavior†

Yukiko Oba,[a] Megumi Okuhata,[a] Toshiyuki Osakai[a] and Tomoyuki Mochida*[a]

In recent years, solvate and protic ionic liquids (ILs) have attracted much attention. We synthesized both types of ILs from alkyl aza-crown ethers (L = *N*-propyl-1-aza-15-crown-5 (L^1) and *N*-$C_6F_{13}C_2H_4$-1-aza-15-crown-5 (L^2)). The solvate ILs [ML][Tf_2N] (M = Na^+, K^+) were solids (T_m = 58–68 °C), whereas the solvate ILs [ML][Tf_2N] (M = Li^+, Ag^+) and protic ILs [HL][Tf_2N] were liquids with low glass transition temperatures. The ILs containing Na ions were more crystalline and exhibited higher melting points than the other ILs. Decomposition temperatures of the protic ILs were higher than those of the solvate ILs. A protic IL with a paramagnetic anion, [HL^1][$FeCl_4$] (T_m = 70.5 °C), was also synthesized and its crystal structure was determined. The solvate ILs [NaL^2][X] (X = $Cl^–$, $CF_3CO_2^–$, $TsO^–$, $PhSO_3^–$) exhibited a lower critical solution temperature (LCST)–type behavior in water. The effects of salt addition on the LCST of L^2 were also investigated. The LCST of these ILs generally increased with increasing hydrophilicity or basicity of the counter anion. This tendency, which is nearly opposite to that of ILs with quaternary onium cations, is ascribed to the amphiphilic nature of the cation. The corresponding protic ILs did not exhibit LCST.

---

[a]*Department of Chemistry, Graduate School of Science, Kobe University, Rokkodai, Nada, Hyogo 657-8501, Japan. E-mail: tmochida@platinum.kobe-u.ac.jp*

†Electronic supplementary information (ESI) available: Raman spectrum of [KL^1][Tf_2N] (Fig.

S1), ^{1}H NMR spectra of L^1 and $[HL^1][Tf_2N]$ (Fig. S2), DSC traces (Fig. S3), TG traces (Fig. S4), Photographs of $[NaL^2][CF_3CO_2]$–water below and above the LCST (Fig. S5), Miscibilities of $[NaL^2]X$ and water (Fig. S6), glass transition temperatures of 1:1 and 1:2 M/L samples (Table S1), and TG data (Table S2). CCDC 1524557 ($[HL^1][FeCl_4]$). For ESI and crystallographic data in CIF or other electronic format, see DOI:

Introduction

Over the past few decades, the synthesis, characterization, and application of ionic liquids (ILs) have been extensively researched.[1] ILs are usually defined as salts with melting point below 100 °C. The majority of ILs are alkyl quaternary onium salts; however, there are a variety of other ILs including protic ILs (synthesized by mixing acids and bases),[2] solvate ILs (containing metal cations solvated with ligands),[3] and metal-containing ILs (including metal complexes as the cation or anion).[4] Solvate ILs can be classified as a subset of metal-containing ILs. Our group has synthesized numerous metal-containing ILs from metallocene derivatives and chelate complexes.[5]

Recently, ILs exhibiting lower critical solution temperature (LCST)–type behavior have attracted significant interest.[6] A typical LCST-type system is a mixture of ILs and water that exhibits phase separation at temperatures above the LCST.[7] This phenomenon is useful for separation and extraction purposes. Aggregation structures of ILs in aqueous solution have been elucidated,[8] and the effect of salts on IL–water extraction systems has been investigated extensively.[9]

In the current study, to develop multifunctional ILs with these useful characteristics, we synthesized ILs using alkyl aza-crown ethers as ligands (Fig. 1). *N*-Propyl-1-aza-15-crown-5 (L^1) and *N*-13-1H,1H,2H,2H-perfluorooctyl-1-aza-15-crown-5 (L^2) were used as the ligands. L^2 is much more hydrophobic than L^1. Of the alkali metal ions, 15-crown-5 ethers capture Na^+

ions most efficiently. We expected that these ligands produce solvate ILs (Fig. 1a) upon incorporation of a metal ion and protic ILs upon protonation of the nitrogen atom (Fig. 1b). This feature enables comparative studies of solvate and protic ILs. Furthermore, this feature is advantageous for ion extraction. Alkyl crown ethers have been used as extracting agents with ILs.[10] Several solvate[11] and onium-based ILs[12] containing crown ether moieties have been reported, although their thermal properties are not well understood. In addition, there seems to be no solvate or protic ILs with LCST behavior reported to date.

This paper reports the synthesis and properties of solvate ILs ([ML][Tf_2N]; M = Li^+, Na^+, K^+, Ag^+; L = L^1, L^2; Tf_2N = bis(trifluoromethanesulfonyl)amide), protic ILs ([HL][Tf_2N]; L = L^1, L^2), and a paramagnetic protic IL ([HL^1][$FeCl_4$]), as shown in Fig. 1. HTf_2N is a superacid (pK_a = −10) and readily forms salts with tertiary amines (pK_a ~ 10).[2c] The thermal properties of these ILs were investigated using differential scanning calorimetry (DSC) and thermogravimetric (TG) analysis. The crystal structure of the paramagnetic protic IL was determined. Furthermore, we found that [NaL^2][X] exhibits LCST-type behavior depending on the anion. The LCST behavior of the salts and ligands was investigated.

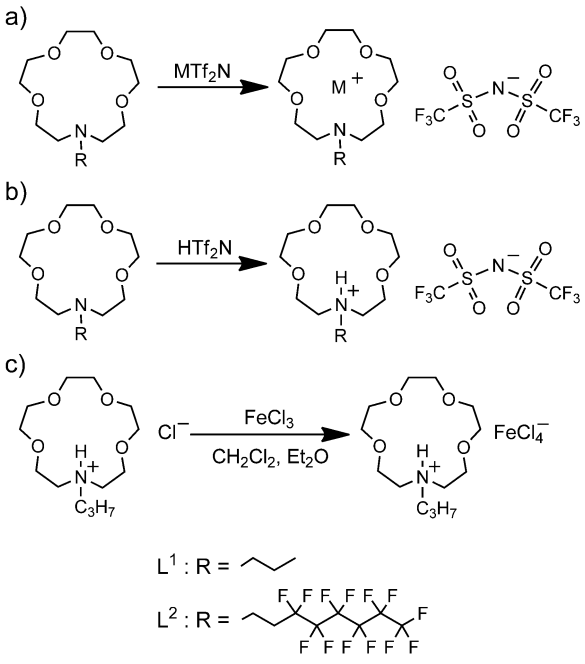

Fig. 1 Synthetic routes to generate ILs from alkyl aza-crown ethers. (a) Solvate ILs, [ML][Tf_2N]

(M = Li^+, Na^+, K^+, Ag^+); (b) protonated ILs, [HL][Tf_2N]; and (c) a paramagnetic protic IL, [HL^1][$FeCl_4$].

Results and Discussion

Syntheses of ILs

Solvate ILs with formulae of [ML][Tf_2N] (M = Na^+, K^+; L = L^1, L^2) were obtained as white solids (T_m = 58–68 °C) upon reaction of the appropriate ligand and M[Tf_2N] in acetone (80–90% yields). The Raman spectrum of [KL^1][Tf_2N] displays peaks corresponding to the *trans* conformation of the anion (Fig. S1, ESI†), whereas alkali metal salts with Tf_2N exhibit the *cis* coformation owing to their chelate coordination.[13] This result is consistent with the coordination of L^1 to the metal ion. Protic ILs with formulae of [HL][Tf_2N] (L = L^1, L^2) were obtained as pale yellow liquids and were prepared by the reaction of the appropriate ligand and HTf_2N in dichloromethane (35% and 82% yields). The shifts of the ^1H NMR peaks were observed upon the formation of PILs, as expected (Fig. S2, ESI†). The metal-containing protic IL, [HL^1][$FeCl_4$] (T_m = 70.5 °C), was synthesized by reacting L^1, HCl, and $FeCl_3$ to generate the desired product as yellow crystals (78% yield).

It has been reported that heating mixtures of crown ethers and alkali metal salts produces metal complexes.[14] Therefore, solvate ILs [ML][Tf_2N] (M = Li^+, Ag^+) were prepared by annealing a 1:1 mixture of the appropriate ligand and M[Tf_2N] at >100 °C for 3 min. Among them, [AgL^2][Tf_2N] may be an equilibrium mixture and not a stoichiometric 1:1 salt, as shown in the thermogravimetry section. Solvate ILs [NaL^2][X] (X = Cl^-, $PhSO_3^-$, TsO^-, $CF_3CO_2^-$) were also prepared using this procedure. They were liquids at room temperature but [NaL^2][CF_3CO_2] crystallized upon heating and melted at T_m = 74.4 °C.

Thermal properties of Tf_2N salts

The melting points, glass transition temperatures, and related parameters for the Tf_2N salts and ligands determined by DSC measurements are listed in Table 1. The corresponding DSC traces are shown in Fig. S3 (ESI†). [ML][Tf_2N] (M = Na^+, K^+; L = L^1, L^2) are solids that melt below 100 °C, whereas [ML][Tf_2N] (M = Li^+, Ag^+) and [HL][Tf_2N] are liquids with glass transitions at low temperatures.

First, the results for [ML][Tf_2N] (M = Na^+, K^+) are discussed. [NaL][Tf_2N] exhibited higher melting points (61.9 °C for L^1 and 68.4 °C for L^2) than [KL][Tf_2N] (59.1 °C for L^1 and 57.9 °C for L^2). The Na complexes crystallized at around 20 °C upon cooling from the melt and exhibited a glass transition under rapid cooling; in contrast, the K complexes only exhibited a glass transition once melted. These tendencies are ascribed to the larger lattice energy and planarity of the Na complexes due to the smaller ionic radius of Na^+ than K^+. The ratio of the glass transition temperature to the melting point for [NaL^1][Tf_2N] was 0.67, which follows the empirical rule ($T_g/T_m = 2/3$),[15] whereas the ratios for the other salts were slightly higher (0.71–0.76).

The glass transition temperatures in [ML][Tf_2N] (M = Li^+, Na^+, K^+, Ag^+), which ranged from −60 to −21 °C, are plotted in Fig. 2 versus the effective ionic radii of the metal ions. The transition temperatures of the alkali metal complexes increase with increasing cation size (ionic radius of Li^+: 78 pm, Na^+: 102 pm, K^+: 138 pm; six-coordination[16]). A similar trend is seen also in onium ILs, in which the glass transition temperatures tend to increase with increasing molecular volumes.[17] The glass transition temperatures of Ag complexes (ionic radius of Ag^+: 116 pm) were similar or slightly lower than those of the Na complexes.

Next, the glass transitions in the protic ILs and the ligands are discussed. The glass transition temperatures of [HL][Tf_2N] were −58 °C (L = L^1) and −37 °C (L = L^2), whereas those of the ligands were −97 °C (L^1) and −83 °C (L^2). The glass transition temperatures of L^2 and its ILs are higher than those of L^1 and its ILs by 14–21 °C. This trend is reasonable considering

the larger molecular volume of L^2. The glass transition temperatures of [HL][Tf_2N] are slightly higher than those of Li complexes, although the ionic radii of H^+ is smaller than that of Li^+. This phenomenon is probably ascribed to hydrogen bonding in [HL][Tf_2N].

To investigate the effect of excess ligands, DSC measurements were performed on 1:2 mixtures of M[Tf_2N] and L^1. They exhibited only glass transitions after annealing, and their glass transition temperatures are also included in Fig. 2. The transition temperatures generally increased with increasing cation size, and those of the 1:2 samples were lower than those of the 1:1 samples by 4–15°C. This tendency seems reasonable considering the low glass transition temperature of the ligand. However, the Ag complexes are exceptional in that the 1:1 and 1:2 samples exhibit comparable glass transition temperatures. This phenomenon is probably due to the diverse coordination abilities of the Ag^+ ion, enhancing intermolecular interactions.[18]

Table 1 Melting point (T_m), melting enthalpy (ΔH), melting entropy (ΔS), glass transition temperature (T_g), and decomposition temperature (T_{dec}) values of the ligands and salts[a]

	T_m (°C)	ΔH (kJ mol^{-1})	ΔS (J K^{-1} mol^{-1})	T_g (°C)	T_{dec}[e]
L^1				−97	(143[f])
[NaL^1][Tf_2N]	61.9	25.0	74.7	−48	288
[KL^1][Tf_2N]	59.1	21.8	65.6	−37	232
[LiL^1][Tf_2N][b]	–[d]			−60	278
[AgL^1][Tf_2N][b]	–[d]			−53	292
[HL^1][Tf_2N]	–[d]			−58	300
[HL^1][$FeCl_4$]	70.5	24.2	70.3		261
L^2				−83	(150[f])
[NaL^2][Tf_2N]	68.4	25.2	73.9	−27	268
[KL^2][Tf_2N]	57.9	22.7	68.5	−21	222
[LiL^2][Tf_2N][b]	–[d]			−43	280
[AgL^2][Tf_2N][b,c]	–[d]			−27	[c]
[HL^2][Tf_2N]	–[d]			−37	272

[a]Determined by DSC measurements (10 K^{-1}min^{-1}). [b]Prepared by annealing a mixture of the ligand and metal salt. [c]Mixture containing a non 1 : 1 M/L complex, exhibiting two-step decomposition at 150 and 250°C. [d]Not observed. [e]Determined by TG measurements (−5 wt%, at 5 K^{-1}min^{-1}). [f]Weight loss due to evaporation.

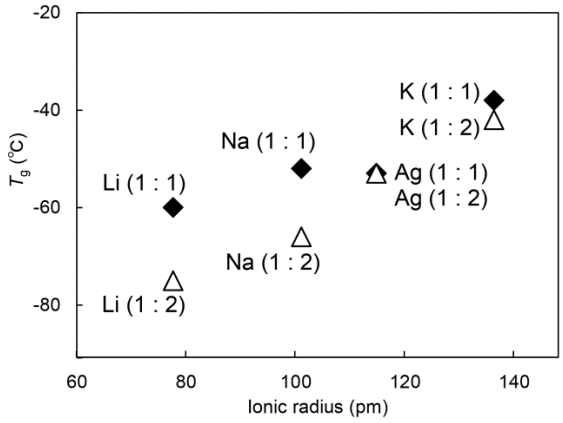

Fig. 2 Plots of the glass transition temperatures (T_g) versus metal ion radii of the 1:1 and 1:2 M/L samples prepared from L^1 and M[Tf_2N] (M = Li^+, Na^+, K^+, Ag^+).

Thermogravimetric analyses of Tf_2N salts

The thermal stabilities of the ILs were investigated by TG analyses. The decomposition temperatures (T_d), which are defined here as the temperatures at which weight losses of 5% occur, are listed in Table 1. Both the solvate and protic ILs exhibited weight losses at much higher temperatures than the ligands, as expected, and the decomposition behavior confirmed 1:1 M/L complexation ratio of the solvate ILs except [AgL^2][Tf_2N]. The protic ILs had higher decomposition temperatures than the solvate ILs.

The TG traces of L^1 and its ILs are shown in Fig. 3. As seen in Fig. 3a, ligand L^1 exhibited significant weight loss at around 150 °C because of evaporation. In contrast, [ML^1][Tf_2N] (M = Li^+, Na^+, K^+) exhibited weight losses at much higher temperatures (T_{dec} = 232–288 °C, Table 1). These occurred in two steps, the first step (41–48% weight loss) corresponding to desorption of the ligand (calculated values: 42–49%; Table S2, ESI†) and the second step corresponding to decomposition of the anion. The results are consistent with the report that heating alkali metal complexes with dibenzocrown ether ligands results in desorption of the ligand.[19] Similarly to the case of L^1, ligand L^2 evaporated at around 150 °C and [ML^2][Tf_2N] (M = Li^+, Na^+, K^+) exhibited a two-step decomposition at higher temperatures (Fig. S4, ESI†). [AgL^1][Tf_2N]

gradually decomposed in one step (Fig. 3b). However, $[AgL^2][Tf_2N]$ exhibited a two-step weight loss at around 150 °C (20% weight loss) and 250 °C (Fig. S4, ESI†). The weight loss at 150 °C suggests the presence of a free ligand, hence this compound may not be a 1:1 salt but an equilibrium mixture.

The decomposition temperatures of $[ML][Tf_2N]$ are summarized in Fig. 4. As seen in the figure, the salts containing L^2 have lower decomposition temperatures than those with L^1, probably because of the weaker intermolecular interactions of the perfluoroalkyl chains. In both series, the decomposition temperature of the Na complex is approximately 50 °C higher than that of the K complex. This phenomenon is ascribed to the larger solvation energy of the smaller Na^+ ion and suitable size of Na^+ for the crown ether ring, which stabilizes the resultant complex. The latter effect is probably responsible for the comparable thermal stability of $[NaL^1][Tf_2N]$ and $[LiL^1][Tf_2N]$ despite the larger ionic radius of Na^+. $[AgL^1][Tf_2N]$ also exhibits a relatively high decomposition temperature.

To confirm the stoichiometry of complex formation, TG measurements were performed on the 1:2 mixtures of $M[Tf_2N]$ ($M = Li^+$, Na^+, K^+, Ag^+) and L^1 after annealing. As shown in Fig. 5, these samples underwent weight loss through evaporation of excess ligand at around 150–230 °C and then exhibited the same decomposition behavior as the 1:1 salts. This result indicates that the products were mixtures of the 1:1 salt and excess ligand. However, in the Ag complex, the ratio of the ligand evaporated was slightly smaller, leaving a complex with a 1:1.1 M/L composition. This retention of excess ligand can be attributed to the diverse coordination ability of Ag^+ ions,[18] which leads to stronger intermolecular interactions. This feature may contributes to the higher decomposition temperature of the Ag complex.

The decomposition temperatures of the protic ILs ($[HL][Tf_2N]$) were 300 °C ($L = L^1$) and 272 °C ($L = L^2$). Again, the IL with L^1 had higher thermal stability than that with L^2. The protic ILs had higher decomposition temperatures than the solvate ILs with the same ligand

([ML^1][Tf_2N]: 232–292°C, [ML^2][Tf_2N]: 222–268°C); this is ascribed to the smaller cation and stabilization through hydrogen bonding. Unlike [ML][Tf_2N], these salts showed a one-step sharp weight loss of nearly 100%, indicating continuous or concomitant evaporation of the ligand and HTf_2N (Fig. 3b). The one-step decomposition behavior is also consistent with the formation of protic ILs, supporting that they are not equilibrium mixtures but stoichiometrically formed 1:1 salts.

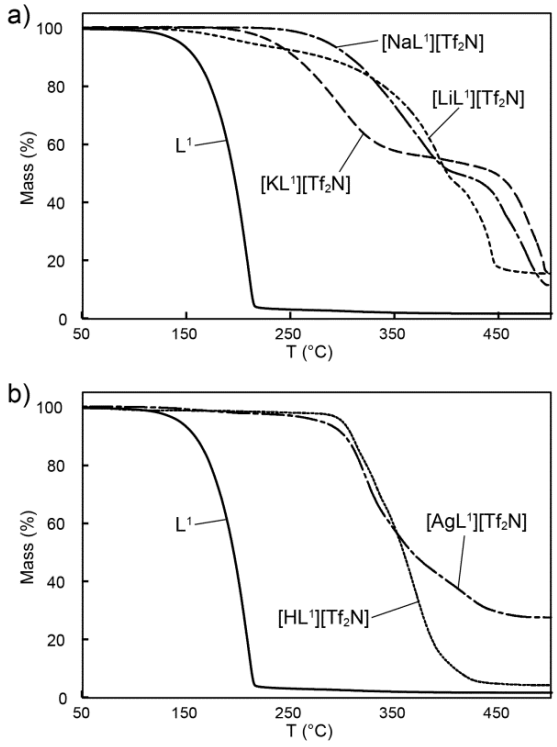

Fig. 3 TG traces of L^1 and its alkali-metal complexes (heating rate: 5 K min^{-1}).

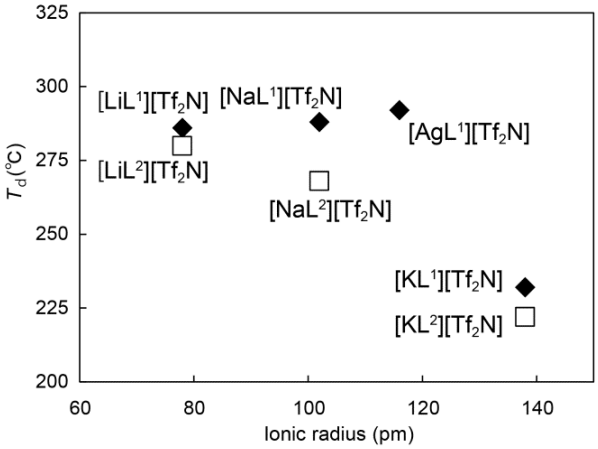

Fig. 4 Plots of the decomposition temperatures of the ILs (−5 wt%, determined by TG

measurements) versus the effective ionic radii of the metal ions. Salts with L^1 and L^2 are represented by closed diamonds (♦) and open squares (□), respectively.

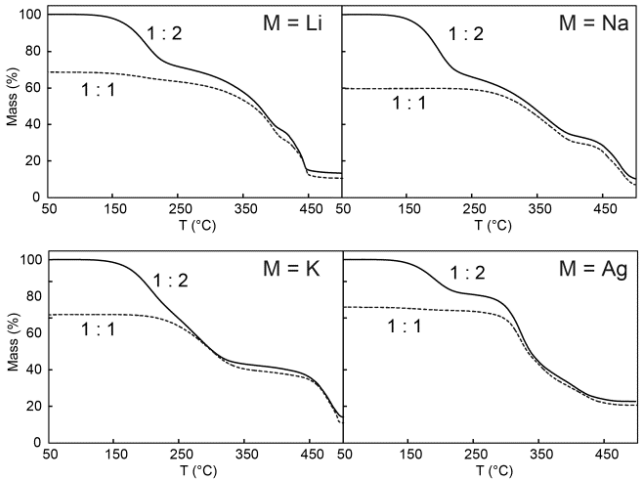

Fig. 5 TG traces of the 1:2 M/L samples prepared from L^1 and M[Tf_2N] (M = Li, Na, K, Ag). Data for the 1:1 complexes ([ML^1][Tf_2N]), normalized by the amount of metal salt, are also indicated (dashed lines).

Thermal properties and crystal structure of [HL^1][$FeCl_4$]

The metal-containing protic IL, [HL^1][$FeCl_4$], was a solid that melts at 70.5 °C (Table 1) and crystallizes upon cooling from the melt at around 60 °C. This melting point is higher than those of the solvate ILs, [ML^1][Tf_2N] (M = Na^+, K^+), by approximately 10 °C, whereas the melting entropies are comparable (ΔS = 70.3 J K^{-1} mol^{-1}; Table 1). This salt underwent a phase transition at 7.0 °C (ΔS = 31.7 J K^{-1} mol^{-1}) in the solid state (Fig. S3d, ESI†).

To confirm the protonated structure of the cation, the crystal structure of this salt was determined using X-ray crystallography at 100 K. This salt crystallized in the space group $P-1$, and the unit cell contained one crystallographically independent molecule. The packing diagram is shown in Fig. 6a. The anions and cations alternate in the crystal, and the anion is located close to the cationic center. The molecular structure of the cation is shown in Fig. 6b. The crown ether ring exhibits extensive disorder over two sites with the occupancy of 2:1. The

propyl group is also disordered over two sites. Despite the lack of conformation freedom of the $FeCl_4$ anion, the melting point and melting entropy of this salt are similar to those of $[ML^1][Tf_2N]$. This is attributed to the ring disorder, which increases the entropy of the solid phase, thereby lowering the melting point.

As shown in Fig. 6b, the crown ether ring is bent and the NH hydrogen is hydrogen-bonded to two oxygen atoms in the ring (N···O distances: 2.82 and 2.85 Å). There are no intermolecular hydrogen bonds. In the crystals of protonated aza-crown ethers, the NH hydrogen often forms hydrogen bonds to the counter anions or solvate water molecules,[20] whereas there are a few salts that have intramolecular hydrogen bonds similar to the present case.[21]

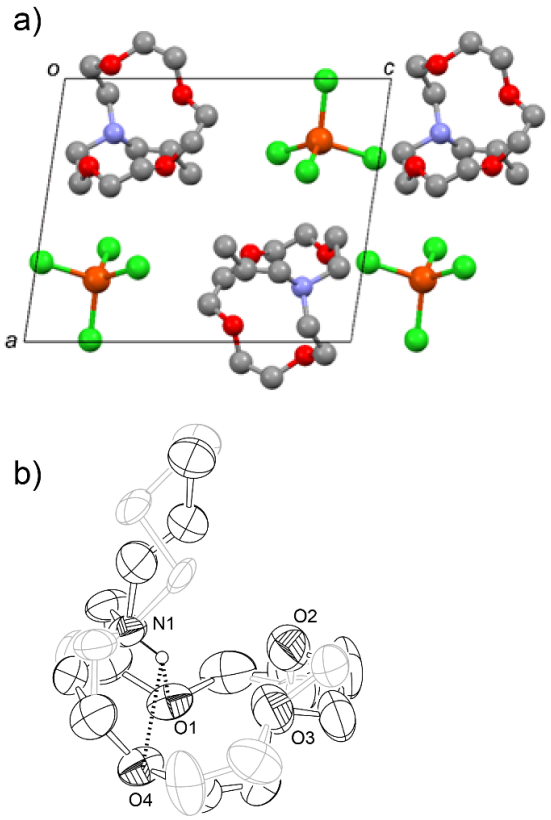

Fig. 6 (a) Packing diagram of $[HL^1][FeCl_4]$ determined at 100 K. Hydrogen atoms and the minor components of the disordered moieties are omitted for clarity. (b) ORTEP drawing of the cation drawn at the 30% probability level. The minor component of the disordered moiety is displayed in gray. The dotted lines represent hydrogen bonds. Hydrogen atoms except for the

NH hydrogen are omitted.

LCST-type behavior of [NaL^2][X]

We investigated the miscibility of solvate ILs [NaL^2][X] and water between 10 and 80 °C, and found that the ILs with X = Cl^-, TsO^-, $PhSO_3^-$, and $CF_3CO_2^-$ exhibit LCST-type behavior in water. The chemical formulae of benzenesulfonate and related anions used are shown in Fig. 7. Photographs of [NaL^2][$PhSO_3$]–water mixture below and above the LCST are shown in Fig. S5 (ESI†). DSC measurements revealed that these ILs exhibit glass transitions at −80, −56, −65, and −22°C, respectively. Among them, [NaL^2][CF_3CO_2] crystallized upon heating at around 45 °C and melted at 74.4 °C (ΔS_m = 49 $JK^{-1}mol^{-1}$).

The miscibility data of [NaL^2][X]–water are summarized in Table 2. Examination of LCST revealed that the anion enhances phase miscibility in the order of Tf_2N^- < Cl^- < $CF_3CO_2^-$ < $PhSO_3^-$ < TsO^- < $MtsO^-$. [NaL^2][Tf_2N]–water exhibited only phase separation. [NaL^2][Cl]–water exhibited phase separation in a 1:1 (w/w) mixture but exhibited LCST in the salt-rich region. In a 1:1 (w/w) mixture, [NaL^2][CF_3CO_2]–water and [NaL^2][$PhSO_3$]–water exhibited LCST at 32 °C and 60 °C, respectively. [NaL^2][TsO]–water exhibited no phase separation in a 1:1 mixture, but it exhibited LCST in the water-rich region. [NaL^2][MtsO] exhibited no phase separation in the corresponding water ratio range.

In contrast to [NaL^2][X], the corresponding protic ILs ([HL^2][X]; X = Cl^-, OTs^-, $CF_3CO_2^-$) were fully miscible with water and did not exhibit LCST. This feature is ascribed to the protonated species being much more hydrophilic than the Na complex.

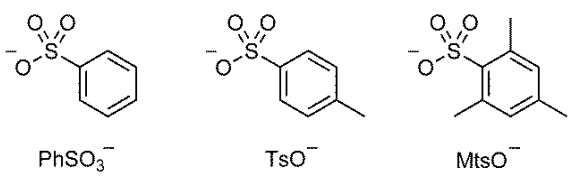

Fig. 7. Benzensulfonate and related anions used for the investigation of LCST phenomena.

Table 2 Miscibilities of [NaL^2]X–water mixtures between 10 and 80 °C (✓: fully miscible, ○: LCST-type behavior, ×: immiscible). LCSTs at specific ratios are also shown in parenthesis.[a]

IL	IL–water ratio (w/w)		
	1:2	1:1	2:1
[NaL^2][Tf_2N]	×	×	×
[NaL^2][Cl]	×	×	○ (50°C[f])
[NaL^2][CF_3CO_2]	×	○ (32°C[d])	✓
[NaL^2][$PhSO_3$]	○ (33°C[b])	○ (60°C[e])	✓
[NaL^2][TsO]	○ (71°C[c])	✓	✓
[NaL^2][MtsO]	✓	✓	–[g]

[a]LCST determined at IL–water ratios (w/w) of [b]1:1.42, [c]1:1.34, [d]1:0.92, [e]1:0.96, and [f]1:0.24. [g]Separation of solid occurred.

LCST-type behavior of L^2 and the effect of salt addition

We further investigated the LCST of the ligand–water mixtures and the effect of salt or acid addition to the mixture. It has been known that various non-ionic surfactants including polyethers[22] and crown ethers[23] exhibit LCST behavior. We found that the L^2–water (1:1 v/v) mixture exhibit a cloud point at 26 °C. A diluted solution of L^2 (10 mM) also exhibited a cloud point at 28 °C. In contrast, L^1 is highly hydrophilic and did not exhibit LCST-type behavior in water.

To investigate the effect of salt addition, the cloud points of 1:1 (v/v) mixtures of L^2 and a 1 M aqueous solution of NaX (X = Tf_2N^-, Cl^-, $CF_3CO_2^-$, $PhSO_3^-$, TsO^-, $MtsO^-$) were investigated. The results are summarized in Table 3. Addition of salts other than $NaTf_2N$ increased the cloud point to 36–61 °C; this feature is ascribed to the salting-in effect caused by complexation of the Na^+ ion to the ligand.[23] The cloud point increased in the order of Cl^- < $CF_3CO_2^-$ < $PhSO_3^-$ < TsO^- < $MtsO^-$. In the case of $NaTf_2N$ addition, however, the cloud point decreased with increasing salt concentration (23.5 °C at 0.1 M and 11 °C at 0.3 M), and the 1

M solution was not miscible with L^2. This behavior is ascribed to the strong hydrophobicity of the Tf_2N anion. Therefore, the order of the anions to increase the LCST of the L^2–water mixture exactly matches the order found for increasing the LCST of $[NaL^2][X]$–water mixtures.

The effect of acid addition (1:1 v/v, 1 M) was also investigated. The mixture of L^2 and an aqueous solution of HTf_2N exhibited only phase separation, whereas the mixtures with solutions of HCl and TsOH exhibited cloud points at 66 and 60 °C, respectively (Table 3). These LCSTs are much higher than those observed for the addition of NaCl or NaTsO (36 and 54 °C, respectively). This is consistent with the higher hydrophilicity of the protonated species versus that of the Na complex.

Table 3 LCSTs of 1:1 (v/v) mixtures of L^2 and aqueous solutions of salts or acids (1 M)

Solute	LCST (°C)
–[a]	26
$NaTf_2N$	–[b], 24[c] (0.1 M), 11[c] (0.3 M)
NaCl	36
$NaCF_3CO_2$	43
$NaPhSO_3$	44
NaTsO	54
NaMtsO	61
HTf_2N	–[b]
HCl	66
TsOH	60

[a]LCST in water. [b]Exhibited phase separation. [c]Measured at indicated concentrations.

Discussion of effect of anions on LCST

The results shown in the previous section demonstrate that the anion enhances phase miscibility in the order of $Tf_2N^- < Cl^- < CF_3CO_2^- < PhSO_3^- < TsO^- < MtsO^-$ in the $[NaL^2][Tf_2N]$–water mixture. It is noteworthy that the observed order is opposite to that for ILs with quaternary onium cations[7a] ($Tf_2N^- < MtsO^- < CF_3CO_2^- < TsO^- < PhSO_3^- < Cl^-$), excepting the fluorine-

containing anions (Tf_2N^- and $CF_3CO_2^-$).

The standard Gibbs energy of ion transfer from water to nitrobenzene ($\Delta G^0_{tr}{}^{W\to O}$/ kJ mol^{-1}, values in parenthesis),[24] which is a measure of the hydrophilicity of the ion, decreases in the order: Cl^- (38.2) > $PhSO_3^-$ (21.0) > TsO^- (18.0) > $MtsO^-$ (16.6). The hydrophilicity index of the anions, determined by Ohno from the water affinity of ILs with quaternary onium cation,[7] is in excellent agreement with this order. The LCST of the quaternary onium ILs simply depends on the water affinity of the anions because the cations are hydrophobic. In the present case, however, the metal-containing cation and the ligand are both amphiphilic and behave as surfactants. Therefore, the effect is likely more dependent on the ability of the anion to stabilize micellar structures below LCST, not on the water affinity of the anion. This idea is further supported by the result that the order of the anions to increase the LCST of the L^2–water mixture was exactly the same as that in the $[NaL^2][Tf_2N]$–water mixture.

The order of the anions to affect the LCST in the present system can be rationalized based on the hydrophobicity of the anion (Hofmeister series[9]) or the basicity of the anion. There are many studies on the anion dependence[25,26] and the effect of salt addition[9,27,28] on the aggregations or micelles of ILs or ionic surfactants in water, which demonstrate that hydrophobic anions are more strongly bound to the surface of micelles and reduce repulsion between the cationic headgroups, to stabilize the micellar structure and thus decrease their critical micelle concentration. This effect is opposite to the water solubility of the anion, hence the reversed order of anion dependence between the present case and ILs with quaternary onium cations is reasonable. The deviation of fluorine-containing anions may be due to the fluorous interaction. Tf_2N^- is strongly hydrophobic hence it seems reasonable that its salts are not miscible with water in the both cases. In addition, the basicity of the anion probably affects the micelle stability. The pK_a values of their conjugated acids (values shown in parenthesis[29]) increase in the order: Tf_2N (-10^{2c}) < HCl (−8) < CF_3CO_2H (0.5) < $PhSO_3H$ (0.7) < TsOH <

MtsOH. This order is in complete agreement with the order observed in the current study. It is reasonable that the more basic anions cause stronger anion binding to stabilize the micelle. To understand the phenomenon in more detail, investigation of anion dependence of the distribution of each component in the two phases above LCST may be important, although the Na^+ ion has a very large binding constant to 15-crown-5 in water.

Conclusions

Solvate ILs ([ML][Tf_2N]; M = Li^+, Na^+, K^+, Ag^+) and protic ILs ([HL][Tf_2N]) with alkyl aza-crown ethers were synthesized. A protic IL with a paramagnetic anion ([HL^1][$FeCl_4$]) was also synthesized and crystallographically characterized. The ILs containing Na ions, which matched the crown ether size, were more crystalline and exhibited higher melting points than the other ILs. The protic ILs exhibited lower glass transition temperatures and greater thermal stability than the solvate ILs. The glass transition temperatures and decomposition temperatures of these ILs tend to correlate with the cation size.

Solvate ILs [NaL^2][X] exhibited LCST behavior in water depending on the anion. The corresponding protic ILs were more hydrophilic and did not exhibit phase separation. Therefore, solvate ILs that exhibit LCST behavior were found. A mixture of L^2 and water also exhibited LCST behavior, and the addition of NaX and HX to this solution increased the cloud point except for the case of the hydrophobic Tf_2N anion. The effect of anions on the LCST is related to the ability of the anion to stabilize the micelles in the mixture and not their solubility. As a result, anion dependence of LCST was nearly opposite to that of ILs with quaternary onium cations.

The knowledge obtained through this study on aza-crown ether–based ILs will be useful for future applications, such as metal-ion extraction, cloud-point extraction, and magnetic separation. It is a great advantage that the physical properties of the ILs can be further tuned by

changing the size of the crown ether ring, counter anion, and substituents to suit the desired applications. Further work will include detailed elucidation of the LCST-type behavior and extraction performance as well as exploration of a novel extraction system.

Experimental Section

General

N-Propyl-1-aza-15-crown-5 (L^1)[30] and N-13-1H,1H,2H,2H-perfluorooctyl-1-aza-15-crown-5 (L^2)[31] were synthesized according to literature methods. ^{1}H NMR spectra were recorded using a Bruker AVANCE 400 spectrometer (400 MHz). DSC measurements were performed using a TA Instruments Q100 differential scanning calorimeter over the temperature range of −150 to 180 °C at a rate of 10 K min^{-1} or other rates if necessary. For the DSC measurements of the mixtures of L^1 and M[Tf_2N] (M = Li^+, Na^+, K^+, Ag^+), the samples were annealed at >100 °C for 3 min to ensure complex formation prior to the measurements. The sample amounts used were 2.93–7.90 mg. IR spectra were acquired via attenuated total reflectance (ATR, diamond) from 550 to 4000 cm^{-1} using a Thermo Nicolet Avatar 360 FT-IR spectrometer. UV-Vis spectra were recorded on a JASCO V-570 UV/VIS/NIR spectrometer. The temperature dependence of the spectra was determined using a CoolSpeK cryostat. TG analyses were performed at a heating rate of 5 K min^{-1} under a nitrogen atmosphere using a Rigaku TG 8120 thermal analyzer. For measurements of the 1:1 or 2:1 L/M samples containing L^1 and M[Tf_2N], the mixtures were heated to 130 °C under a nitrogen atmosphere and then annealed for 3 min to ensure complex formation and evaporation of water. Raman spectra were acquired at room temperature using an NRS-7100 laser Raman spectrometer (532 nm excitation).

The LCST behavior of the ionic liquid–water mixtures was visually observed in an oil bath using a mixture of approximately 10 mg of L^2, the corresponding amount of salt, and various volumes of water. The LCST behavior of the L^2–water mixture was investigated as

follows: The ligand and an aqueous solution of metal salts or acids (1:1 v/v) were injected into a capillary (1.6 mm o.d.) and stored at 10 °C for several days, during which the capillary was rotated several times to ensure uniform mixing. The resultant uniform solutions were used to observe the LCST. The cloud points were determined using an SRS melting point apparatus (MPA100) at a heating rate of 1 °C min^{-1} up to 80 °C. The cloud point was defined as the temperature at which the reflectance became 50% of that of the phase-separated state. The cloud point of L^2 in water at 10 mM was determined using UV-vis spectrometry by determining the temperature at which the transmittance at 550 nm reached 50%.

Syntheses of complexes with L^1

[HL^1][Tf_2N]. Dichloromethane solutions of L^1 (50.1 mg, 0.20 mmol) and HTf_2N (58 mg, 0.21 mmol) were mixed, evaporated under reduced pressure, and washed with water three times. The organic layer was dried over magnesium sulfate, and the solvent was evaporated under reduced pressure. The product was obtained as a pale yellow oil (37.4 mg, 35% yield), which further dried under vacuum at 80 °C for 3 h. ^{1}H NMR ($CDCl_3$): δ = 1.04 (t, 3H, J = 7.43 Hz), 1.78–1.84 (m, 2H), 3.22–3.27 (m, 2H), 3.50–3.52 (m, 4H), 3.59–3.71 (m, 10H), 3.73–3.81 (m, 4H), 3.88–3.95 (m, 2H). Anal. Calcd. for $C_{15}H_{28}O_8F_6N_2S_2$: C, 33.21; H, 5.20; N, 5.16. Found: C, 32.98; H, 5.14; N, 5.38. IR (cm^{-1}): 570, 614, 653, 739, 751, 788, 937, 1053, 1130, 1181, 1226, 1349, 1461, 2881.

[NaL^1][Tf_2N]. Acetone solutions of L^1 (42.9 mg, 0.164 mmol) and Na[Tf_2N] (60.6 mg, 0.200 mmol) were mixed, and the solvent was evaporated under reduced pressure. Addition of dichloromethane to the solution resulted in the precipitation of unreacted Na[Tf_2N], which was removed by filtration. The solvent was then evaporated under reduced pressure. The resultant oil was dissolved in a dichloromethane–hexane mixture (1:1), and the solution was slowly cooled to −40 °C. The desired product precipitated as a white solid (73.6 mg, 79% yield), which

was collected by filtration and dried under vacuum at room temperature for a few hours. ^{1}H NMR (DMSO-d_6): δ = 0.88 (t, 3H, J = 7.31 Hz), 1.41–1.50 (m, 2H), 2.54–2.58 (m, 2H), 2.67 (t, 4H, J = 4.77 Hz), 3.53 (t, 4H, J = 4.77 Hz), 3.61–3.70 (m, 12H). Anal. Calcd. for $C_{15}H_{27}O_8F_6N_2NaS_2$: C, 31.92; H, 4.82; N, 4.96. Found: C, 31.71; H, 4.62; N, 5.09. IR (cm^{-1}): 570, 605, 646, 741, 762, 787, 944, 998, 1056, 1112, 1124, 1181, 1226, 1243, 1333, 1481, 2880.

[KL^1][Tf$_2$N]. This salt was prepared using the same method as for [NaL^1][Tf$_2$N] using L^1 (50.1 mg, 0.20 mmol) and K[Tf$_2$N] (67.0 mg, 0.21 mmol). The product was obtained as a white solid (92.2 mg, 84% yield) after storing the resultant oil at −40 °C. The solid was collected and dried under vacuum. ^{1}H NMR (DMSO-d_6): δ = 0.88 (t, 3H, J = 7.30 Hz), 1.40–1.51 (m, 2H), 2.43–2.47 (m, 2H), 2.60 (s, br, 4H), 3.04–3.55 (m, 5H), 3.55–3.78 (s, br, 11H). Anal. Calcd. for $C_{15}H_{27}O_8F_6N_2KS_2$: C, 31.03; H, 4.69; N, 4.82. Found: C, 31.20; H, 4.89; N, 4.92. IR (cm^{-1}): 569, 609, 741, 762, 791, 822, 851, 935, 1001, 1054, 1083, 1103, 1118, 1130, 1179, 1226, 1303, 1332, 1352, 1480, 2879.

[HL^1][FeCl$_4$]. A solution of 5 M HCl aq. (0.2 mL) in diethyl ether (2 mL) was added dropwise to a solution of L^1 (30 mg, 0.11 mmol) in diethyl ether (1 mL). Evaporation of the solvent followed by drying *in vacuo* resulted in a yellow oil. A solution of anhydrous FeCl$_3$ (22.4 mg, 0.14 mmol) in THF (2 mL) was added dropwise to a solution of the obtained oil in dichloromethane (2 mL). After stirring for 1 h, the solvent was removed under reduced pressure. The residue was dissolved in acetonitrile, and, after the addition of diethyl ether, the solution was stored at −40 °C. Yellow crystals of [HL^1][FeCl$_4$] precipitated (39.7 mg, 78% yield). Anal. Calcd. For $C_{13}H_{28}Cl_4FeNO_4$: C, 33.94; H, 6.13; N, 3.04. Found: C, 33.91; H, 6.04; N, 3.15. IR (cm^{-1}): 3100, 2870–2940, 1127, 1081, 924.

[HL^1][FeCl$_4$] was also prepared by reacting L^1 and FeCl$_3$ as follows: Anhydrous FeCl$_3$ (80.2 mg, 0.47 mmol) was dissolved in THF (2 mL), and any undissolved materials were removed by filtration. A solution of L^1 (57.2 mg, 0.22 mmol) in THF (2 mL) was added

dropwise to this solution, and the mixture was stirred for 1 h. After removal of the solvent under reduced pressure, the residue was washed with diethyl ether, dissolved in dichloromethane, and filtered. The filtrate was evaporated and dried under vacuum to give $[HL^1][FeCl_4]$ as a yellow powder. The product was purified by diffusion of diethyl ether into a dichloromethane solution (39 mg, 39% yield). The analytical data for the product were identical with those of the samples prepared using the other method described.

Synthesis of complexes with L^2

$[HL^2][Tf_2N]$. Dichloromethane solutions of L^2 (31.6 mg, 0.06 mmol) and HTf_2N (27.5 mg, 0.10 mmol) were mixed, evaporated under reduced pressure, and washed with water three times. The organic layer was separated and dried over magnesium sulfate. The solvent was evaporated under reduced pressure to give the desired product as a yellow oil (35 mg, 82% yield), which was further dried under vacuum at 80 °C for 3 h. ^{1}H NMR ($CDCl_3$): δ = 2.64–2.82 (m, 2H), 3.45–3.95 (m, 22H). Anal. Calcd. for $C_{20}H_{25}O_8F_{19}N_2S_2$: C, 28.38; H, 2.98; N, 3.31. Found: C, 28.56; H, 3.15; N, 3.42. IR (cm^{-1}): 570, 617, 653, 697, 708, 739, 789, 846, 934, 1055, 1132, 1183, 1230, 1350, 1471, 2878.

$[NaL^2][Tf_2N]$. Acetone solutions of L^2 (97.7 mg, 0.17 mmol) and $Na[Tf_2N]$ (554 mg, 0.18 mmol) were mixed and stirred for 20 min, and the solvent was evaporated under reduced pressure. The residue was dissolved in dichloromethane, and unreacted $Na[Tf_2N]$ was removed by filtration. The filtrate was evaporated under reduced pressure, and the resultant pale yellow oil was stored at −40 °C resulting in precipitation of the desired product as a white solid (130.9 mg, 89% yield), which was further dried under vacuum for a few hours. ^{1}H NMR (DMSO-d_6): δ = 2.16 (m, 2H), 2.65 (m, 4H), 2.96 (m, 2H), 3.50 (t, 4H, J = 4.34 Hz), 3.60 (s, 12H). Anal. Calcd. for $C_{20}H_{24}O_8F_{19}N_2NaS_2$: C, 27.66; H, 2.79; N, 3.23. Found: C, 27.96; H, 2.57; N, 3.44. IR (cm^{-1}): 572, 582, 596, 653, 695, 721, 741, 790, 853, 897, 941, 1000, 1058, 1080, 1133, 1184,

1234, 1326, 1344, 1479, 2878.

[KL^2][Tf$_2$N]. This salt was prepared using the same method as for [NaL^2][Tf$_2$N] using L^2 (48.3 mg, 0.09 mmol) and K[Tf$_2$N] (34.2 mg, 0.11 mmol) except that the resultant pale yellow oil was cooled to −40 °C and then stored at 15 °C. The desired product precipitated as pale yellow crystals (61.8 mg, 82% yield). ^{1}H NMR (DMSO-d_6): δ = 2.25 (m, 2H), 2.66 (m, 4H), 2.97 (m, 2H), 3.54 (t, 4H, J = 4.28 Hz), 3.65 (s, 12H). Anal. Calcd. for $C_{20}H_{24}O_8F_{19}KN_2S_2$: C, 27.16; H, 2.73; N, 3.17. Found: C, 27.43; H, 2.64; N, 3.34. IR (cm^{-1}): 570, 609, 741, 762, 791, 822, 851, 935, 1001, 1054, 1083, 1103, 1118, 1130, 1179, 1226, 1303, 1332, 1352, 1480, 2879.

X-Ray structure determination

X-Ray diffraction data for [HL^1][FeCl$_4$] were collected on a Bruker APEX II Ultra CCD diffractometer using MoKα radiation (λ = 0.71073 Å) at 100 K. Single crystals suitable for structure determination were obtained by diffusion of diethyl ether into a dichloromethane solution of the complex. The structures were determined by direct methods using SHELX-97,[32] and ORTEP-3 for Windows[33] was used to generate the molecular graphics. Crystallographic data at 100 K: $C_{13}H_{28}Cl_4FeNO_4$, M = 460.01, triclinic, P−1, a = 9.6258(16) Å, b = 10.1155(17) Å, c = 12.305(2) Å, α = 109.255(2)°, β = 94.577(2)°, γ = 100.770(2)°, V = 1098.2(3) Å^3, Z = 2, 5677 reflections collected, 4104 independent reflections, 371 parameters, R_1 = 0.0509, wR_2 = 0.1228 ($I > 2\sigma$), R_1 = 0.0834, wR_2 = 0.1412 (all data).

Acknowledgements

This work was financially supported by KAKENHI (grant number 16H04132) from the Japan Society for the Promotion of Science (JSPS). We thank Dr. Y. Funasako (Tokyo Univ. Sci., Yamaguchi) for his help with the X-ray structure analysis.

References

1. *(a)* A. Stark and K. R. Seddon, in *Kirk–Othmer Encyclopedia of Chemical Technology*, Vol. 26, Wiley-Interscience, New York, 5th ed., 2007, pp. 836–919; *(b) Ionic Liquids; Industrial Applications to Green Chemistry*, ed. R. D. Rogers and K. R. Seddon, ACS symposium series, American Chemical Society, Washington, D.C., 2002, vol. 818; *(c)* M. Armand, F. Endres, D. R. MacFarlane, H. Ohno, and B. Scrosati, *Nat. Mater.*, 2009, **8**, 621–629; *(d)* I. Krossing, J. M. Slattery, C. Daquenet, P. J. Dyson, A. Oleinikova and H. Weingärtner, *J. Am. Chem. Soc.*, 2006, **128**, 13427–13434; *(e)* H. Weingärtner, *Angew. Chem., Int. Ed.*, 2008, **47**, 654–670; *(f)* N. V. Plechkova and K. R. Seddon, *Chem. Soc. Rev.*, 2008, **37**, 123–150; *(g)* X. Sun, H. Luo and S. Dai, *Chem. Rev.*, 2012, **112**, 2100–2128.

2. *(a)* T. L. Greaves and C. J. Drummond, *Chem. Rev.*, 2008, **108**, 206–237; *(b)* M. Hasani, J. L. Yarger and C. A. Angell, *Chem. Eur. J.*, 2016, **22**, 13312–13319; *(c)* M. S. Miran, H. Kinoshita, T. Yasuda, M. A. B. H. Susan and M. Watanabe, *Phys. Chem. Chem. Phys.*, 2012, **14**, 5178–5186; (*d*) A. Noda, A. B. Susan, K. Kudo, S. Mitsushima, K. Hayamizu and M. Watanabe, *J. Phys. Chem. B*, 2003, **107**, 4024–4033; (*e*) M. Yoshizawa, W. Xu and C. A. Angell, *J. Am. Chem. Soc.*, 2003, **125**, 15411–15419.

3. *(a)* C. A. Angel, Y. Ansari and Z. Zhao, *Faraday Discuss*., 2012, **154**, 9–27; *(b)* W. A. Henderson, F. McKenna, M. A. Khan, N. R. Brooks, V. G. Young, Jr. and R. Frech, *Chem. Matter.*, 2005, **17**, 2284–2289; *(c)* K. Ueno, K. Yoshida, M. Tsuchiya, N. Tachikawa, K. Dokko and M. Watanabe, *J. Phys. Chem. B*, 2012, **116**, 11323–11331; *(d)* T. Mandai, K. Yoshida, K. Ueno, K. Dokko and M. Watanabe, *Phys. Chem. Chem. Phys.*, 2014, **16**, 8761–8772; *(e)* T. Muephy, S. K. Callear, N. Yepuri, K. Shimizu, M. Watanabe, J. N. C. Lopes, T. Darwish, G. G. Warr and R. Atkin, *Phys. Chem. Chem. Phys.*, 2016, **18**, 17224–17236.

4. *(a)* J. Klingele, *Coord. Chem. Rev.*, 2015, **292**, 15–29; *(b)* Y. Yoshida and G. Saito, Progress in Paramagnetic Ionic Liquids, in Ionic Liquids; Theory, Properties, New Approaches, ed. A. Kokorin, InTech, 2011, pp. 723–738; *(c)* N. R. Brooks, S. Schaltin, K. Van Hecke, K. Van Meervelt, K. Binnemans and J. Fransaer, *Chem.-Eur. J.*, 2011, 17, 5054–5059; *(d)* A. Branco, L. C. Branco and F. Pina, *Chem. Commun.*, 2011, **47**, 2300–2302; *(e)* M. Iida, C. Baba, M. Inoue, H. Yoshida and E. Furusho, *Chem. -Eur. J.*, 2008, **14**, 5047–5056; *(f)* J. F. Huang, H. M. Luo and S. Dai, *J. Electrochem. Soc.*, 2006, **153**, J9–J13; *(g)* P. Zhang, Y. Gong, Y. Lv, Y. Guo, Y. Wang, C. Wang and H. Li, *Chem. Commun.*, 2012, **48**, 2334–2336; *(h)* P. Nockemann, B. Thijs, N. Postelmans, K. Van Hecke, L. Van Meervelt and K. Binnemans, *J. Am. Chem. Soc.*,

2006, **128**, 13658–13659; *(i)* B. Mallick, B. Balke, C. Felser and A. -V. Mudring, *Angew. Chem., Int. Ed.*, 2008, **47**, 7635–7638; *(j)* R. J. Brown, P. J. Dyson, D. J. Ellis, T. Welton and *Chem. Commun.*, **2001**, 1862–1863; *(k)* I. J. B. Lin and C. S. Vasam, *J. Organomet. Chem.*, 2005, **690**, 3498–3512; *(l)* H. D. Pratt III, A. J. Rose, C. L. Staiger, D. Ingersoll and T. M. Anderson, *Dalton Trans.*, 2011, **40**, 11396–11401.

5. *(a)* T. Inagaki and T. Mochida, *Chem. Lett.*, 2010, **39**, 572–573; *(b)* Y. Funasako, T. Mochida, T. Inagaki, T. Sakurai, H. Ohta, K. Fukukawa and T. Nakamura, *Chem. Commun.*, 2011, **47**, 4475–4477; *(c)* T. Inagaki and T. Mochida, *Chem. Eur. J.*, 2012, **18**, 8070–8075; *(d)* Y. Funasako, S. Mori and T. Mochida, *Chem. Commun.*, 2016, **52**, 6277–6279; *(e)* Y. Funasako, T. Mochida, K. Takahashi, T. Sakurai and H. Ohta, *Chem. Eur. J.*, 2012, **18**, 11929–11936; *(f)* M. Okuhata, Y. Funasako, K. Takahashi and T. Mochida, *Chem. Commun.*, 2013, **49**, 7662–7664; *(g)* X. Lan, T. Mochida, Y. Funasako, K. Takahashi, T. Sakurai and H. Ohta, *Chem. Eur. J.*, 2017, **23**, 823–831.

6. *(a)* H. Glasbrenner and H. Weingärtner, *J. Phys. Chem.*, 1989, **93**, 3378–3379; *(b)* J. Jacob, M. A. Anisimov, J. V. Segers, A. Oleinikova, H. Weingärtner and A. Kumar, *Phys. Chem. Phys. Chem.*, 2001, **3**, 829–831; *(c)* J. Łachwa, J. Szydlowski, V. N. Visak, L. P. N. Rebelo, K. R. Seddon, M. N. da Ponte, J. M. S. S. Esperança and H. J. R. Guedes, *J. Am. Chem. Soc.*, 2005, **127**, 6542–6543; *(d)* J. Łachwa, J. Szydlowski, K. R. Seddon, M. S. S. Esperança, H. J. R. Guedes and L. P. N. Rebelo, *Green Chem.*, 2006, **8**, 262–267; *(e)* K. Fukumoto and H. Ohno, *Angew. Chem. Int. Ed.*, 2007, **46**, 1852–1855; *(f)* F. Käfer, F. Liu, U. Stahlschmidt, V. Jérôme, R. Freitag, M. Karg and S. Agarwal, *Langmuir*, 2015, **31**, 8940–8946.

7. *(a)* Y. Kohno, H. Arai, S. Saita and H. Ohno, *Aust. J. Chem.*, 2011, **64**, 1560–1567; *(b)* Y. Kohno and H. Ohno, *Phys. Chem. Chem. Phys.*, 2012, **14**, 5063–5070; *(c)* H. Ohno, K. Fujita, and Y. Kohno, *Phys. Chem. Phys. Chem.*, 2015, **17**, 14454–14460; *(d)* S. Saita, Y. Kohno and H. Ohno, *Chem. Commun.*, 2013, **49**, 93–95.

8. *(a)* J. Łuczak, J. Hupka, J. Thöming and C. Jungnickel, *Colloids Surf. A: Physicochem. Eng. Aspects*, 2008, **329**, 125–133; *(b)* R. Wang, W. Leng, Y. Gao and L. Yu, *RSC. Adv*., 2014, **4**, 14055–14062.

9. D. Dupont, D. Depuydt and K. Binnemans, *J. Phys. Chem. B*. 2015, **119**, 6747–6757.

10. *(a)* S. Dai, Y. H. Ju and C. E. Barnes, *J. Chem. Soc., Dalton Trans*., 1999, 1201–1202; *(b)* S. Chun, S. V. Dzyuba and R. A. Bartsch, *Anal. Chem.*, 2001, **73**, 3737–3741; *(c)* H. Luo, S. Dai and P. V. Bonnesen, *Anal. Chem*., 2004, **76**, 2773–2779; *(d)* A. E. Visser, R. P. Swatloski, W. M. Reichert, S. T. Griffin and R. D. Rogers, *Ind. Eng. Chem. Res.*, 2000, **39**, 3596–3604; *(e)* H. Zhao, S. Xia and P. Ma, *J. Chem. Technol. Biotecnol.*, 2005, **80**, 1089–1096; *(f)* F. Yang,

Z. Jiao, Z. Huang, J. Xie and H. Guo, *J. Incl. Phenom. Macrocycle. Chem.*, 2012, **74**, 257–263; *(g)* K. Kurahashi, S. Umetani and Y. Sohrin, *Anal. Sci.*, 2008, **24**, 225–229; *(h)* O. A. Fedorova, F. Maurel, A. V. Chbun'kova, Y. P. Strokach, T. M. Valova, L. G. Kuzmina, J. A. K. Howard, M. Wenzel, K. Gloe, V. Lokshin and A. Samat, *J. Phys. Org. Chem.*, 2007, **20**, 469–483.

11. *(a)* S. Dai and H. Luo, *USPatent* 7, 423,164 B2, 2003; *(b)* Y. Song, H. Jing, B. Li and D. Bai, *Chem. Eur. J.*, 2012, **17**, 8731–8738; *(c)* Y. Song, C. Cheng and H. Jing, *Chem. Eur. J.*, 2014, **20**, 12894–12900; *(d)* G. He, K. Kikukawa, N. Nishiyama, H. Ohe and T. Matsuda, *Bull. Chem. Soc. Jpn.*, 1988, **61**, 3785–3787; *(e)* J. Shu, P. Xie, D. Lin, R. Chen, J. Wang, B. Zhang, M. Liu, H. Liu and F. Liu, *Anal. Chim. Acta*, 2014, **806**, 152–164.

12. *(a)* X. Zhou, P. Xie, J. Wang, B. Zang, M. Liu, H. Liu and X. Feng, *J. Chromatogr. A,* 2011, **1218**, 3571–3580; *(b)* M.-C. Tseng, T.-C. Yuan, Z. Li and Y.-H. Chu, *Anal. Chem.*, 2016, **88**, 10811–10815.

13. S. Ntais, A. M. Moschovi, F. Paloukis, S. Neophytides, V. N. Burganos, V. Dracopoulos, V. Nikolakis, *J. Power Sources*, 2011, **196**, 2202–2210.

14. *(a)* R. E. A. Dillon, C. L. Stern and D. F. Shriver, *Chem. Mater*., 2001, **13**, 2516–2522; *(b)* A. D. S. Gomes, C. M. F. Oliveira, *Thermochim. Acta*, 1976, **17**, 107–111.

15. *(a)* D. Tombull and M. H. Cohen, *Modern Aspect of the Vitreous State*; Butterworth: London, 1960; Vol. *1*, p 38; *(b)* O. Yamamuro, Y. Minamimoto, Y. Inamura, S. Hayashi and H. Hamaguchi, *Chem. Phys. Lett.*, 2006, **423**, 371–375.

16. R. D. Shannon, *Acta Cryst.* 1976, **A32**, 751–767.

17. W. Xu, E. I. Cooper and C. A. Angell, *J. Phys. Chem. B*, 2003, **107**, 6170–6178.

18. P. D. Prince, J. W. Steed and P. J. Cragg, *Chem. Commun*., 1999, 1179–1180.

19. G. Pokol, B. Ágai, T. M. T. Tran, I. Bitter, L. Töke and S. Gál, *Thermochim. Acta*, 1998, **319**, 87–95.

20. *(a)* M.S. Fonari, V. C. Kravtsov, Y. A. Simonov, S. S. Basok, E. V. Ganin, V. O. Gelmboldt, K. Suwinska, J. Lipkowski, O. A. Alekseeva and N.G. Furmanova, *Poluhedron*, 2008, **27**, 2049–2058; *(b)* K. R. Fewings and P. C. Junk, *Aust. J. Chem.*, 1999, **52**, 1109–1114; *(c)* J. Rebizant, M. R. Spirlet, P. P. Barthelemy and J. F. Desreux, *Acta Crystallogr.*, 1987, **C43**, 909–912.

21. T. Gunnlaugsson, M. Nieuwenhuyzen, L. Richard and V. Thoss, *J. Chem. Soc., Perkin Trans.*, 2002, **2**, 141–150.

22. *(a)* C. Ren, W. Tian, I. Szleifer and Y. Ma, *Macromolecules*, 2011, **44**, 1719–1727; *(b)* R. Carabias-Martínez, E. Rodríguez-Gonzalo, B. Moreno-Cordero, J. L. Pérez-Pavón, C. García-Pinto and E. F. Laespada, *J. Chromatogr. A*, 2000, **902**, 251–265.

23. *(a)* I. Ikeda, H. Emura and M. Okahara, *Bull. Chem. Soc. Jpn.*, 1984, **57**, 1612–1616; *(b)* Effect of metal salts on the cloud point of alkyl crown compounds, M. Okahara, P.-L. Kuo, S. Yamamura and I. Ikeda, *J. Chem. Soc., Chem. Commun*., 1980, 586–587.
24. *(a)* W. Murakami, K. Eda, M. Yamamoto and T. Osakai, *J. Electroanal. Chem.*, 2013, **704**, 38–43; *(b)* T. Osakai, Y. Naito, K. Eda and M. Yamamoto, *J. Phys. Chem. B*, 2015, **119**, 13167–13176.
25. *(a)* B. Dong, N. Li, L. Zheng, L. Yu and T. Inoue, *Langmuir*, 2007, **23**, 4178–4182; *(b)* H. Wang, J. Wang, S. Zhang and Z. Zuan, *J. Phys. Chem. B*, 2008, **112**, 16682–16689.
26. N. Jiang, P. Li, Y. Wang, J. Wang, H. Yan and R. K. Thomas, *J. Colloid Interface Sci*., 2005, **286**, 755–760.
27. H. Wang, Q. Feng, J. Wang and H. Zhang, *J. Phys. Chem. B*, 2014, **114**, 1380–1387.
28. K. Maiti, D. Mitra, S. Guha and S. P. Moulik, *J. Mol. Liq*., 2009, **146**, 44–51.
29. (*a*) *CRC Handbook of Chemistry and Physics*, 84th ed., editor-in-chief: D. R. Lide, CRC Press, Boca Raton, 2003; (*b*) G. Bordwell, *Acc. Chem. Res.,* 1988, *21*, 456–463.
30. S. Elshani, E. Kobzar and R. A. Bartsch, *Tetrahedron*, 2000, **56**, 3291–3301.
31. H. Shimizu, Y. Nakatsuji and O. Okahara, JP-1997-2700158.
32. *(a)* G. M. Sheldrick, *Acta Cryst.*, 2015, **A71**, 3–8; *(b)* G. M. Sheldrick, *Acta Cryst.*, 2015, **C71**, 3–8.
33. L. J. Farrugia, *J. Appl. Crystallogr.*, 1999, **32**, 837–838.

Table of contents entry

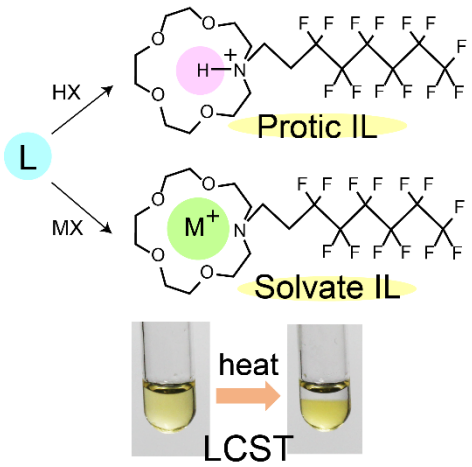

Solvate and protic ILs containing alkyl aza-crown ethers were synthesized, some of which exhibited an LCST–type behavior in water.

Supporting Information

Solvate and protic ionic liquids from aza-crown ethers: synthesis, thermal properties, and LCST behaviour

Yukiko Oba,[a] Megumi Okuhata,[a] Toshiyuki Osakai[a] and Tomoyuki Mochida*[a]

[a]*Department of Chemistry, Graduate School of Science, Kobe University, Rokkodai, Nada, Hyogo 657-8501, Japan. E-mail: tmochida@platinum.kobe-u.ac.jp*

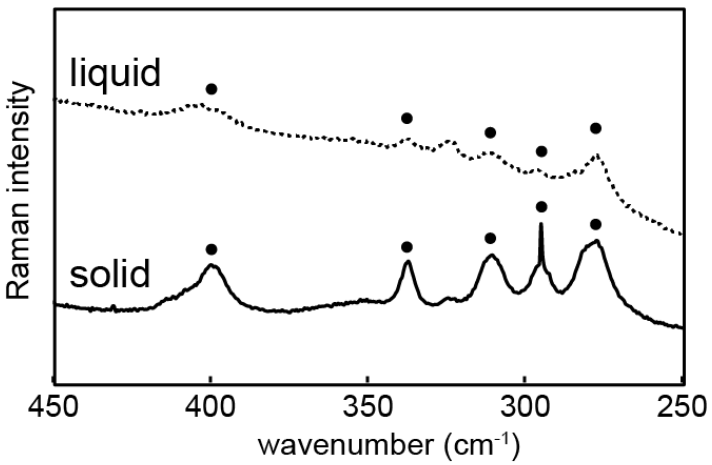

Fig. S1. Raman spectra of [KL^1][Tf_2N] at room temperature in the solid state (solid line) and supercooled liquid state (dotted line). The filled circles indicate the peaks corresponding to the *trans* form of the Tf_2N anion.

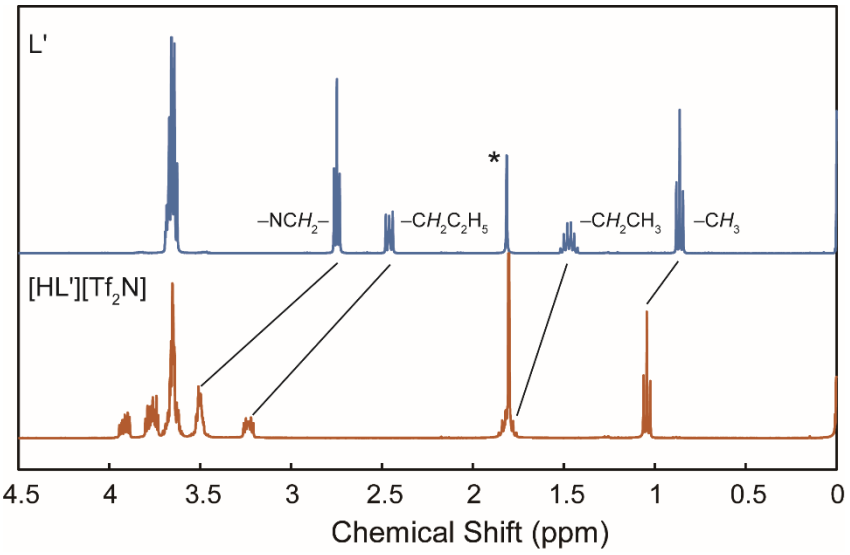

Fig. S2 ^{1}H NMR spectra of L^{1} and $[L^{1}][Tf_2N]$ measured in $CDCl_3$.

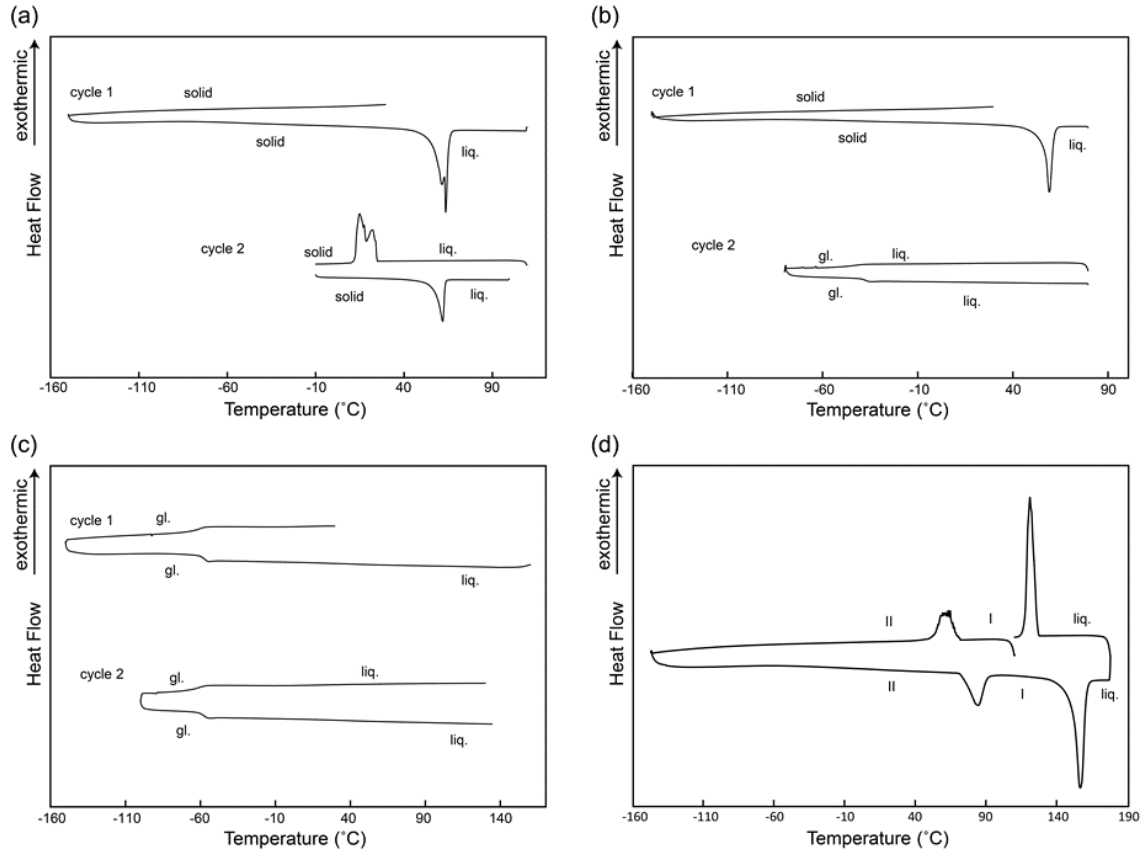

Fig. S3 DSC traces of (a) $[NaL^{1}][Tf_2N]$, (b) $[KL^{1}][Tf_2N]$, (c) $[HL^{1}][Tf_2N]$, and (d) $[HL^{1}][FeCl_4]$.

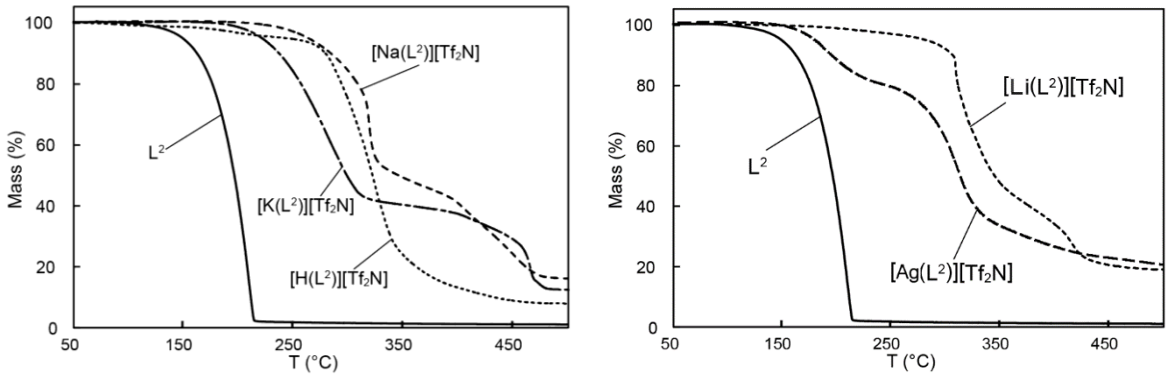

Fig. S4 TG traces of L^2 and its complexes (heating rate: 5 K min^{-1}).

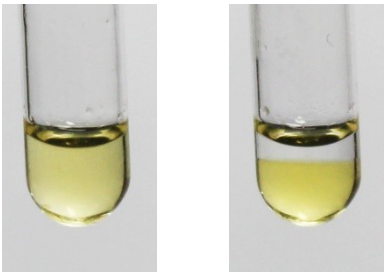

Fig. S5. Photographs of $[NaL^2][CF_3CO_2]$–water mixture below the LCST (left) and above the LCST (right).

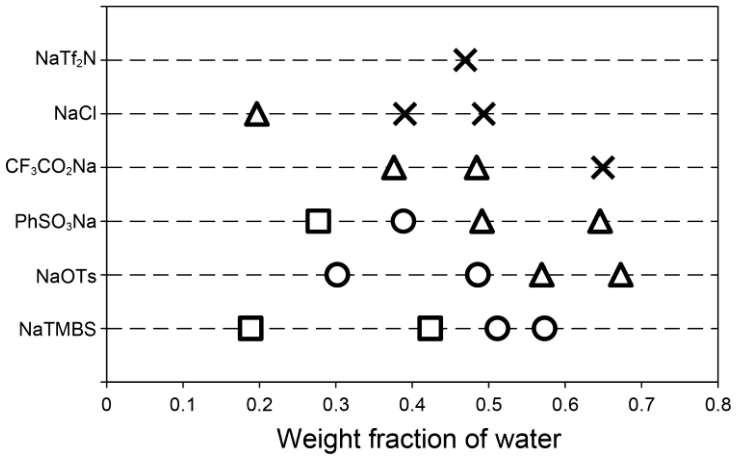

Fig. S6. Miscibilities of $[NaL^2]X$ and water between 10 and 80 °C plotted versus water content (○: fully miscible, △: LCST-type behavior, ×: immiscible, □: separation of solid). Sodium salts used to prepare the ILs are shown on the left.

Table S1 Glass transition temperatures (T_g) of 1:1 and 1:2 M/L samples prepared by annealing of mixtures of L^1 and M[Tf_2N]

M	M : L	T_g (°C)
Li	1 : 1	–60
	1 : 2	–75
Na	1 : 1	–52
	1 : 2	–66
K	1 : 1	–38
	1 : 2	–42
Ag	1 : 1	–53
	1 : 2	–53

Table S2 Decomposition temperatures (T_d) and weight losses in the first step (m_{exp}) of ILs determined by TG measurements. Calculated values of weight loss by the loss of ligand (m_{calc}) are also shown

	T_d (°C)[a]	m_{exp} (%)	m_{calc} (%)
[HL^1][Tf_2N]	300	–[c]	
[LiL^1][Tf_2N][b]	286	48	49.4
[NaL^1][Tf_2N]	288	48	46.3
[KL^1][Tf_2N]	232	41	45.0
[AgL^1][Tf_2N][b]	292	37	41.5
[HL^2][Tf_2N]	272	–[c]	
[NaL^2][Tf_2N]	268	47	65.1
[KL^2][Tf_2N]	222	59	63.9

[a]–5wt% (heating rate: 5 K min^{-1}). [b]Prepared by annealing the mixtures of ligand and metal salt. [c]Continuous weight loss.